IEEE Access
Multidisciplinary | Rapid Review | Open Access Journal

Received October 13, 2020, accepted November 1, 2020, date of publication November 9, 2020, date of current version November 19, 2020.

Digital Object Identifier 10.1109/ACCESS.2020.3036846

Design and Analysis of Preload Control for Space Debris Impact Adhesion Capture Method

ZHENGYOU XIE, XINLONG CHEN, YAJING REN, AND YANGYANG ZHAO
Qian Xuesen Laboratory of Space Technology, Beijing 100094, China
Corresponding author: Zhengyou Xie (xiezhengyou@qxslab.cn)

ABSTRACT The growing space debris poses a serious threat to the safety of the space environment, and the necessity and urgency of active space debris removal have reached a consensus around the world. As one of the key technologies for debris removal, space debris capture has received extensive attention from researchers. In this paper, a space debris impact adhesion capture method is proposed, which involves a device integrated with gecko-inspired adhesion material at the front end and connected to the service spacecraft via a tether. The device can be launched from the service spacecraft, collides with the debris target and adheres to the debris surface to capture. The method provides the advantages of standoff distance allowed, high compatibility with different shaped targets and almost no risk of generating new debris. In order to provide a suitable preload for the adhesives, the device is put forward with a variable damping magnetorheological fluid buffer which could adjust the damping force in real time during the impact process to achieve reliable adhesion capture. The damping force fuzzy control method using impact force and remaining buffer stroke as input is designed. The simulations are carried out and the results show the effectiveness of the preload control method, thus proving a promotion for space debris impact adhesion capture method.

INDEX TERMS Space debris capture, impact adhesion, preload control, magnetorheological fluid buffer, fuzzy control.

I. INTRODUCTION

The dramatic increase in the amount of space debris poses a great safety threat and orbital pollution to the space environment. The space debris have an impact on the smooth conduct of space missions, the normal operation of spacecraft and the safety of astronauts. Even with the cessation of the launch of new spacecrafts, the amount of space debris will increase as a result of ongoing collisions. Therefore, the active debris removal (ADR) has become increasingly important and has received attention from countries and researchers all over the world [1], [2].

Numerous ADR schemes and technologies have been proposed [3]–[5], all of which have their own advantages and drawbacks, and specific application scenarios. Among them, harpoon scheme is considered an attractive capturing method because of its compatibility with different shaped targets, allowed standoff distance and no need of grappling points [2]. Dudziak *et al.* [6] have conducted a lot of experiments and simulation analysis on the ground, which proved the effectiveness of the harpoon scheme. Harpoon capturing method is also one of the concepts from RemoveDEBRIS mission which was the first mission to successfully demonstrate in-orbit. In the mission, technologies for the capture of large space debris by using a harpoon have been triumphantly tested [7], [8]. However, the harpoon has a potential risk of generating more debris as a result of collisions. It may be a good option to change the harpoon to the adhesive mechanism and use adhesion capture instead of puncture capture. The implementation process of adhesion capture method is similar to that of the harpoon scheme. The capture device is launched from the service satellite and adhered to the debris target through impact. Since the capture speed is fast, it is relatively insensitive to the dynamic state of the target and orbital dynamics [9]. It has the same advantages as the harpoon method demonstrates but much lower risk of generating new debris.

The gecko-inspired materials have been extensively researched in recent years, which not only have the features of high adhesion, repeated adhesion-desorption and self-cleaning, but also can adapt to the surface of various material morphology without any damage to the surface, thus

The associate editor coordinating the review of this manuscript and approving it for publication was Giambattista Gruosso.

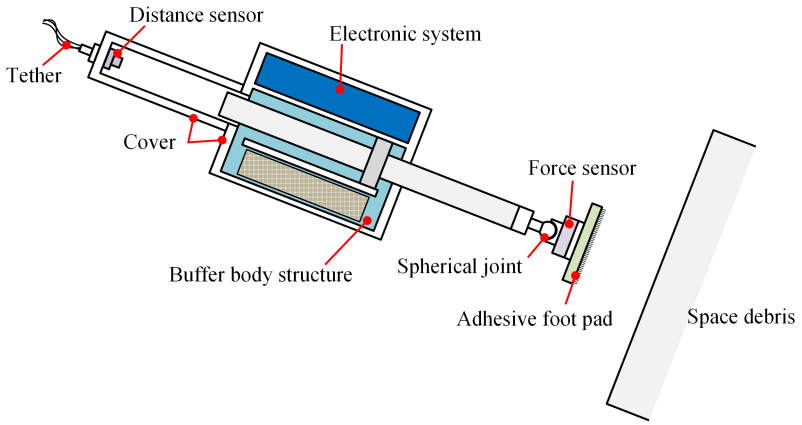

FIGURE 1. Schematic diagram of adhesion capture device.

providing a wide range of application prospects in space [10], [11]. Jiang *et al.* [12] developed a robotic device using gecko-inspired adhesives which can grasp and manipulate large objects in microgravity. Bylard *et al.* [10] have proposed a number of concepts for applying controllable dry adhesives to the challenging problem of reliable rocket bodies debris deorbiting. In these schemes, a robotic arm is usually required to implement zero-distance capture. In this paper, an attempt is made to achieve adhesion capture of debris by launching the device at a distance, thereby improving the convenience and security.

The adhesion properties of gecko-inspired adhesives are often related to the preload, and in some cases, too high or too low preload is not conducive to optimal adhesion [13], [14]. Therefore, the design of a buffer mechanism is necessary in the impact adhesion capture device. On the one hand, the buffer could control the impact force in a desired range in order to provide a suitable preload for adhesives, while being able to extend the action time of the preload to a certain extent, which can be expected to improve the adhesion effect. On the other hand, the buffer can also absorb the collision energy to prevent from contact surface damage. In order to achieve the ability to capture different debris targets in orbit many times, adaptability and repeatability are necessary. In this paper, a controllable buffer is designed based on the magnetorheological fluid (MRF). The MRF has features such as fast response, continuous adjustability, and good controllability, which makes it draw wide concern [15], [16]. Wang *et al.* [17] designed a lunar lander based on MRF and conducted a simulation analysis to verify the ability of MRF to adapt to different landing conditions.

In this paper, an attempt is made to propose a space debris impact adhesion capture method based on MRF buffer and bionic adhesion material. A relevant device is put forward which can be launched from the service satellite and adhered to debris target through impact. Moreover, a fuzzy control strategy is designed to achieve a suitable preload for better adsorption and capture effect. Co-simulations based on Adams and Simulink are carried out under different initial conditions and have verified the validity of the method.

II. SCHEME DESIGN

A. OVERALL STRUCTURE

The space debris adhesion capture device based on magnetorheological fluid (MRF) buffer is illustrated in Fig. 1 The device mainly consists of an adhesive foot pad, a MRF buffer, a force sensor, a distance sensor, and an electronic system including a microcontroller, a power supply unit, and a signal acquisition and transmission circuit. The adhesive foot pad is connected to the device body via a spherical joint, which provides the foot with some adaptability to the inclined landing surface. The force sensor is installed between the foot pad and the spherical joint to measure the contact force during impact adhesion. The distance sensor is integrated to measure the displacement of the piston rod of the buffer to determine the current buffer distance. The real-time force and buffer distance information are used as inputs to the controller during the impact process to achieve optimized preload and reliable adsorption.

The device is tethered to a service satellite platform. When a large space debris needs to be captured, the device would be launched from the satellite to capture the target by means of adhesion. Then, the satellite will pull the debris to a graveyard orbit afterwards.

B. PARAMETERS DESIGN

1) BASIC PARAMETERS

As mentioned above, numerous studies have been carried out on gecko adhesive mechanism and materials. After the material is manufactured, preload is one of the main factors that affects the adsorbability in practice. There is usually a drop in adhesion at high applied preload, and the impact force acts as the preload during adhesion capture. In this paper, the preload and adhesion data from [13] are used for conceptual and structural design. In [13] it was found that for PDMS adhesion material an adhesion maximum of 60 kPa was

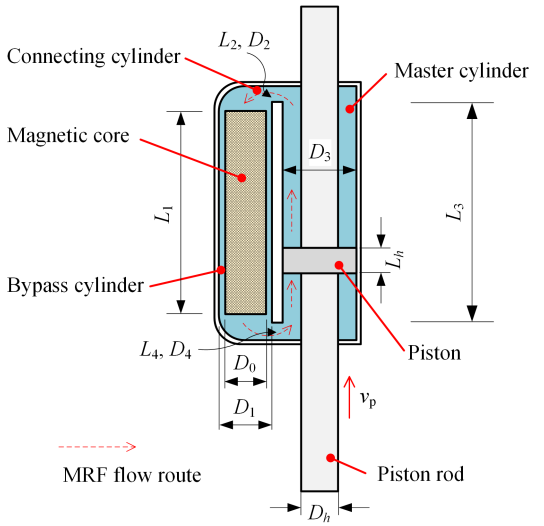

FIGURE 2. Model and dimensions of MRF buffer.

realized for applied stress between 3 and 125 kPa, whereas for preload larger than 125 kPa, very low adhesion strength of 1.2 kPa was recorded.

In order to gain reliable ability during deorbiting manoeuvre, adsorption capacity of 100 N is set as the design target. Thus, the area of the adhesive foot pad should reach 16.67 cm^2 under the maximum adsorption intensity. Considering the possible loss of effective adsorption area caused by the unevenness of the target and other factors, the foot pad is designed with a diameter of 6 cm and an area of 28.27 cm^2, and the theoretical adsorption force could reach 169.6 N. As a result, the preload, that is the impact force, should not exceed the upper limit F_{Limit}.

$$F_{Limit} = 125 \times 28.27 \times 10^{-4} \times 10^3 = 353.4N \quad (1)$$

Moreover, the adhesion capture device is designed to have a mass of no more than 3 kg with an ability to be launched from the satellite at a distance with a velocity of 3-4 m/s to achieve impact adhesion.

2) BUFFER STRUCTURE PARAMETERS

Based on the theorem of kinetic energy and impulse and the preload requirements, as well as considering the size of the device structure, the maximum buffer stroke is determined not more than 100 mm, and the maximum buffer force not less than 300 N.

In this paper, the MRF buffer is designed in a double-ended bypass type as illustrated in Fig. 2. It mainly includes a master cylinder with inner diameter D_3 and equivalent length L_3, a piston rod with diameter D_h, a piston with thickness L_h, a bypass cylinder with inner diameter D_1 and equivalent length L_1, a magnetic core with diameter D_0, and two connecting cylinders with equivalent diameter D_2, D_4 and equivalent length L_2, L_4, respectively.

Assuming that the current speed of piston rod is v_p and the flow rate is Q, the damping forces in each region can be calculated according to [17]. Wherein, the damping force generated in the master cylinder area is

$$F_3 = \frac{32\mu\,(L_3 - L_h)}{(D_3 - D_h)^2} Q \quad (2)$$

$$Q = \frac{\pi\left({D_3}^2 - {D_h}^2\right)}{4} v_p \quad (3)$$

where μ is the MRF viscosity.

The damping force of the bypass cylinder is

$$F_1 = \frac{12\mu L_1}{d^2} Q + \frac{3}{2}\pi L_1 \tau_y\,(D_1 + D_0) \quad (4)$$

where, d is the unilateral clearance between the bypass cylinder and the magnetic core and $d = \frac{D_1 - D_0}{2}$. τ_y is the MRF yield stress under the current magnetic field strength.

The damping forces of the two connecting cylinders are

$$F_2 = F_4 = \frac{32\mu L_2}{{D_2}^2} Q \quad (5)$$

According to Eq. (2)-(5), the total damping force F_{buf} can be obtained as

$$\begin{aligned} F_{buf} &= F_1 + F_2 + F_3 + F_4 \\ &= \frac{3}{2}\pi L_1 \tau_y\,(D_1 + D_0) \\ &\quad + \left(\frac{48\mu L_1}{(D_1 - D_0)^2} + \frac{64\mu L_2}{{D_2}^2} + \frac{32\mu\,(L_3 - L_h)}{(D_3 - D_h)^2}\right) \\ &\quad \times \frac{\pi\left({D_3}^2 - {D_h}^2\right)}{4} v_p \\ &= F_a + F_p \end{aligned} \quad (6)$$

It can be seen that the total damping force consists of two parts: one part varies with the MRF yield stress τ_y and is called F_a which can be actively controlled; and the other part named F_p is the passive damping force and related to the fluid velocity v_p. The τ_y is affected by the magnetic field strength applied to the bypass cylinder. By varying the coil current, the magnetic field strength is changed, which in turn changes the τ_y, ultimately achieving the purpose of adjusting the active damping force F_a.

By examining the design requirements, the main structural parameters of the MRF buffer designed in this paper are shown in Table 1. The magnetorheological fluid product type of MRF-132DG from Lord Company is used as an example in this paper, which has viscosity μ of 0.112 pa.s and maximum yield stress of 48 kPa. Thus, the active and passive damping forces of the buffer are

$$\begin{cases} F_a = 0.01281\tau_y \\ F_p = 58.3v \end{cases} \quad (7)$$

When the yield stress τ_y is at its maximum, there is $F_{a-max} = 614.9N$ and the buffering capacity can meet the requirements.

TABLE 1. Main structural parameters of MRF buffer.

Symbol	Value
L_3	120
D_3	30
D_h	15
L_h	10
L_2, L_4	20
D_2, D_4	12
L_1	80
D_1	18
D_0	16

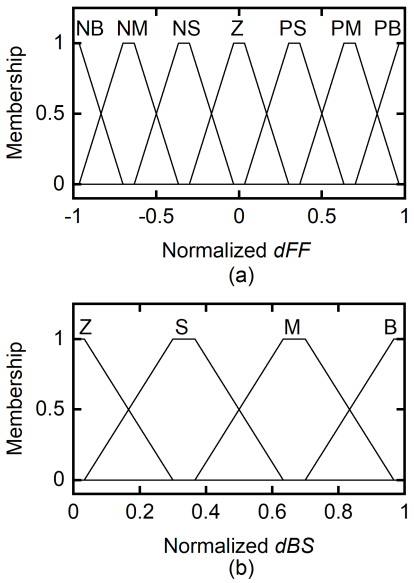

FIGURE 3. Membership affiliations of input (a) *dFF* and (b)*dBS*.

III. CONTROL METHOD FOR MRF BUFFER DAMPING FORCE

Since the impact process is short and complex, it is difficult to establish an accurate model of the MRF buffer under impact load. The fuzzy control method does not need an accurate model, but only requires to formulate control rules based on experience and calculate the control quantity by using fuzzy reasoning which has strong robustness [17]. Furthermore, its fuzzy decision and defuzzification can be offline, which shortens the control time and realizes the real-time control. Thus, the fuzzy control method is adopted to adjust the damping force during impact adhesion.

Set the contact force between foot pad and debris at some point during the impact process to F_{cot}, and the buffer distance to S_b. In this article, take the difference dFF ($dFF = F_{tar} - F_{cot}$) between the contact force F_{cot} and the desired contact force F_{tar}, and the remaining buffer stroke dBS ($dBS = BS_{\max} - S_b$, $BS_{\max}$ ($= 100mm$) is the maximum buffer distance) as inputs of the fuzzy controller. The output is the active damping force F_a of the buffer. In practical application, the control of the active damping force F_a is achieved by controlling the magnetic core coil current.

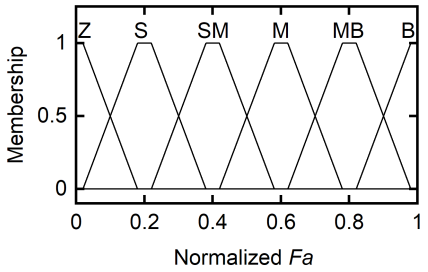

FIGURE 4. Membership affiliations of output F_a.

TABLE 2. Fuzzy control rules for inputs and outputs.

Output:F_a		dBS			
		Z	S	M	B
dFF	NB	S	S	Z	Z
	NM	SM	S	Z	Z
	NS	SM	SM	S	Z
	Z	M	S	S	Z
	PS	M	SM	SM	S
	PM	MB	MB	M	SM
	PB	B	B	MB	M

Considering the control accuracy and efficiency, the input dFF is divided into 7 fuzzy sets NB, NM, NS, Z, PS, PM, PB and the dBS is divided into 4 fuzzy sets Z, S, M, B. Also, the output F_a is divided into 6 fuzzy set Z, S, SM, M, MB, B. The trapezoidal distribution is chosen as the affiliation function of the input and output. The membership affiliations after normalization are shown in Fig. 3 and Fig. 4.

The principles for control rules are established based on experience. When the actual contact force F_{cot} is much lower than the expected preload F_{tar} (that is, dFF belongs to PB) and the remaining buffer stroke dBS is small (S), the output active damping force F_a is big (B), and while dBS is big (B), F_a is Middle (M). When F_{cot} is higher than F_{tar}, at the same time there is still large remaining buffer stroke, the damping force F_a is zero (Z), and while dBS is small (S), F_a is small (S). Detailed fuzzy control rules for inputs and outputs are shown in Table 2.

IV. PRELOAD CONTROL ANALYSIS DURING IMPACT PROCESS

A. SIMULATION METHOD AND CONDITION

Simulation studies of preload control during impact adhesion process are carried out based on MSC Adams and MATLAB/Simulink. A simplified model was established in Adams firstly, which consist of three parts. The masses of the device body, piston rod and foot pad are 2.5 kg, 0.3 kg and 0.1 kg, respectively, and the debris mass is set at 300 kg. A translational joint is established between the piston rod and the body structure, and a spherical joint is set up between the piston rod tip and the foot pad. Also,

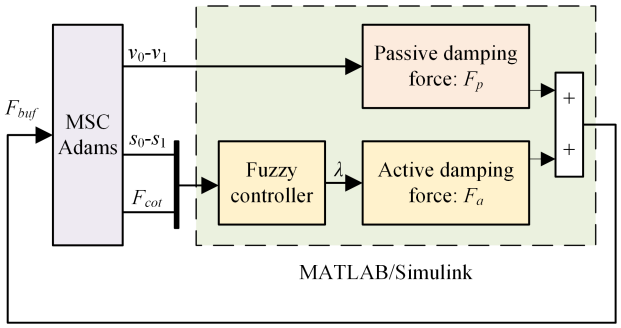

FIGURE 5. Co-simulation control model schematic.

an IMPACT-Function-based contact is created between the foot pad and the debris with the stiffness of 3000 N/mm, force exponent of 1.1, damping factor of 0.6 Ns/mm and penetration depth of 0.1 mm.

In Adams, the real-time velocities (v_0, v_1) and displacements (s_0, s_1) of the device body and the piston rod, and the contact force Fcot are extracted. Then, the relative velocity v ($v = v_0 - v_1$) can be obtained to further calculate the passive damping force F_p of the MRF buffer, and the relative displacement s ($s = s_0 - s_1$) is achieved to characterize the current buffer stroke. The extracted variables are sent to the Simulink controller and compute the total damping force F_{buf}. Then the force is returned to Adams for the next step simulation. The schematic of co-simulation control model is demonstrated in Fig. 5. Eq. (7) shows the composition of the damping force F_{buf}, where λ ($\lambda \in [0,\ 1]$) is the normalized output of the fuzzy controller. In the simulation, the active damping force F_a of the MRF buffer is set to a maximum of 400 N, which does not exceed the maximum buffering capacity.

$$F_{buf} = F_a + F_p = 400\lambda sign\,(v_0 - v_1) + 58.3\,(v_0 - v_1) \quad (8)$$

B. SIMULATION RESULTS ANALYSIS

A series of simulation tests with different impact conditions have been carried out. The simulation results with impact velocity of 4 m/s are exhibited in Fig. 6 which shows the variation curves of the fuzzy controller output λ, active and passive damping forces F_a and F_p, impact force (contact force) F_{cot} and buffer stroke s during impact process. The device collides vertically into the debris target at 0.0027 s. It can be seen that the peak of the contact force F_{cot} reaches 368N in the instant of impact which exceeds the desired value (the desired contact force F_{tar}, that is desired preload of the adhesive foot, is set to 300 N in the simulation). At this moment, the buffer stroke $s = 0$, then the output of the fuzzy controller is close to zero, as a result, the active damping force of the MRF buffer is very small. As the collision proceeds, the fuzzy controller adjusts the output at all times, so that the contact force F_{cot} remains more constant at around 270 N, which can provide an appropriate preload for reliable adhesive capture. The entire impact buffering process lasts 0.039 s and the buffer distance reaches 73.9 mm.

It should be noted that the above results are obtained in the case of simulation step of 0.0001 s, however, the response time of MRF is limited and the step time cannot be set too short. As the MRF response time is in the ms level, the simulation step is set to 0.002 s in Simulink and the results in the same impact condition are obtained as shown in Fig. 7. Due to the delay effect of MRF, the active damping force would not respond well and in real time to the control requirements, and there will be some fluctuation in the impact force. However, it is relatively constant in general, remaining in the range of 200-300 N, which is adequate for the task.

Fig. 8 shows the simulation results with impact velocity of 5 m/s. At the beginning of the collision, the contact force reaches 450 N, but soon drops to 300 N due to the fuzzy controller and remains almost constant. The buffer stroke reaches 97 mm which is close to the maximum value, indicating that the device will no longer meet the requirements when the impact speed is further increased. Of course, when the desired contact force F_{tar} is set higher in the fuzzy controller, the buffer would be able to absorb more collision energy, but the device will not capture the debris reliably due to excessive preload.

V. DISCUSSION FOR MULTI-ADHESIVE FOOT STRUCTURE

Although the single-adhesive foot scheme is simple in structure, it is relatively low in reliability. In order to further enhance the reliability of adhesion capture, it is a good attempt to design a multi-adhesive foot structure to achieve multi-point impact and adhesion. Multiple adhesive feet allow the capture mechanism to adapt to larger debris or the debris with more complex surfaces. Moreover, the adhesion area increases, which can effectively improve capture capacity.

A. MULTI-ADHESIVE FOOT SCHEME AND IMPACT CONDITIONS

A capture mechanism with three adhesive foot pads was designed, and Adams and Simulink continued to be used to carry out preload control analysis of each foot pad during the impact. The simplified model built in Adams is shown in Fig. 9. Three legs with adhesive feet which have the same structure as that in Fig. 1 are connected with the main body through connecting rods. The whole mechanism can be folded up and unfolded. When unfolded, the three adhesive foot pads uniformly distributed in the radius of 200 mm on the circumference.

Three complex cases, including impact target with step surface (see Fig. 9 (a)) and slope surface (see (b) and (c)), were presented for analysis and discussion as listed in Table 3. In these three cases, the feet do not collide with the target at the same time, thus requiring individual damping force control for each adhesive foot. The fuzzy control method described earlier is still used with real-time contact force and buffer stroke of each adhesive foot as control inputs.

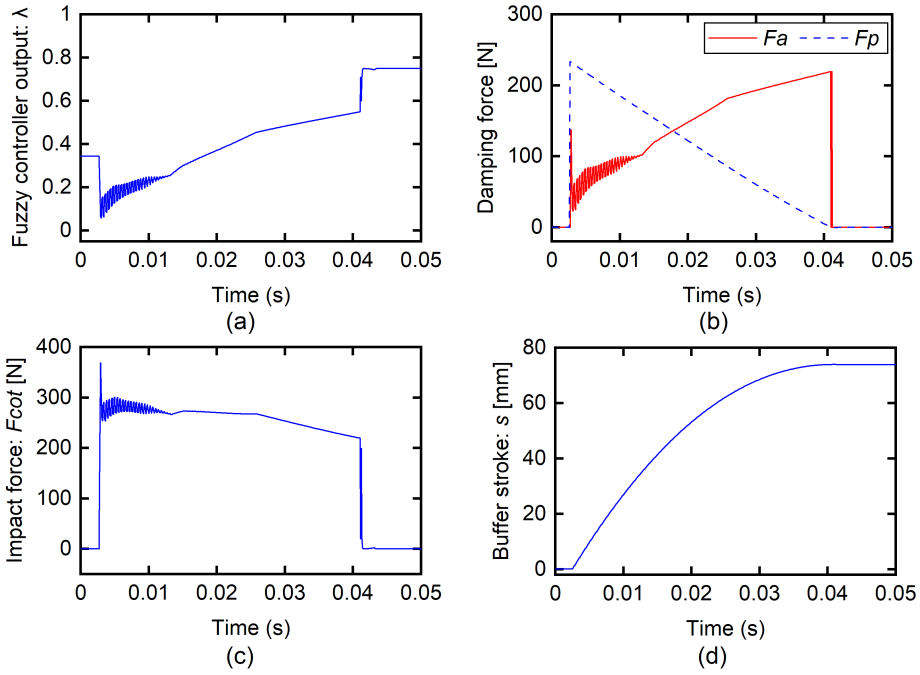

FIGURE 6. Simulation results with impact velocity of 4 m/s. (a) The output of fuzzy controller λ, (b) active and passive damping forces: F_a and F_p, (c) impact force F_{cot}, (d) buffer stroke s.

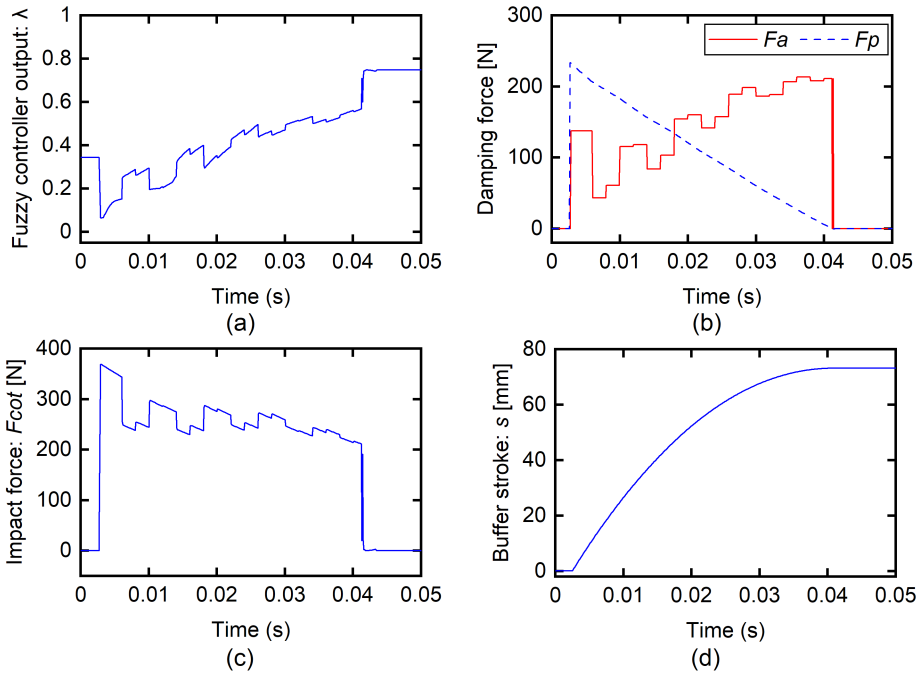

FIGURE 7. Simulation results with impact velocity of 4 m/s and step of 0.002 s. (a) The output of fuzzy controller λ, (b) active and passive damping forces: F_a and F_p, (c) impact force F_{cot}, (d) buffer stroke s.

B. MULTI-ADHESIVE FOOT STRUCTURE IMPACT ANALYSIS

Figure 10 shows the simulation results of the multi-adhesive foot capture device impacts step surface process with 1-2 condition. At $t_1 = 0.0045$ s moment, the foot pad 1, P1 for short, first contacts with the target surface, then after 0.005 s, at t_2 the foot pad 2 and 3, P2 and P3 for short, start to impact the target. Due to the existence of step surface, the device body would have a slight tilt after t_1, which leads the edges of P2 and P3 to collide the target first at t_2. The edge impact effect results in a transient peak contact force F_{cot}

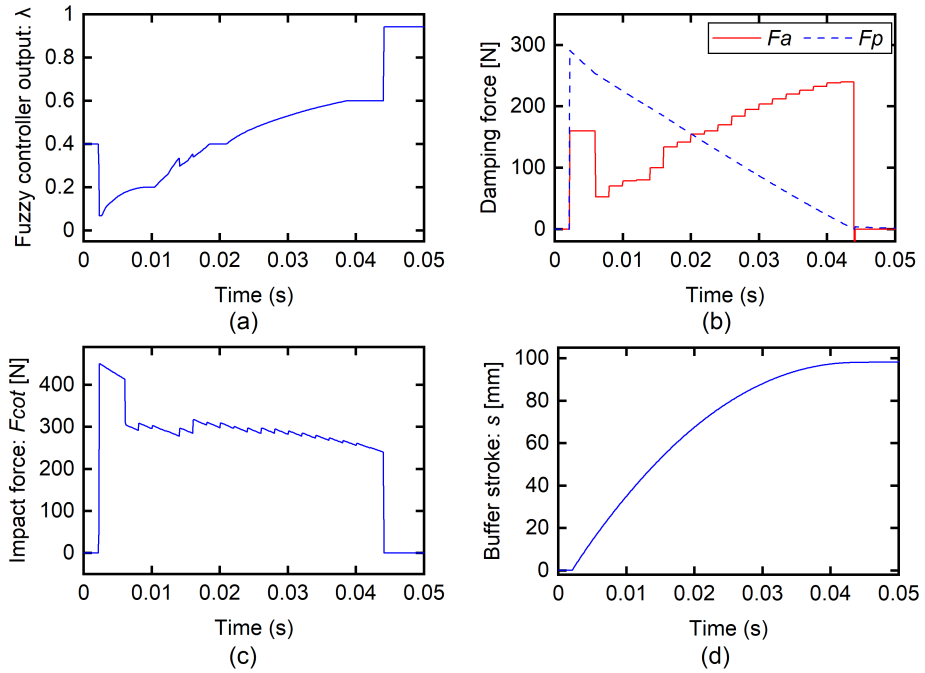

FIGURE 8. Simulation results with impact velocity of 5 m/s and step of 0.002 s. (a) The output of fuzzy controller λ, (b) active and passive damping forces: F_a and F_p, (c) impact force F_{cot}, (d) buffer stroke s.

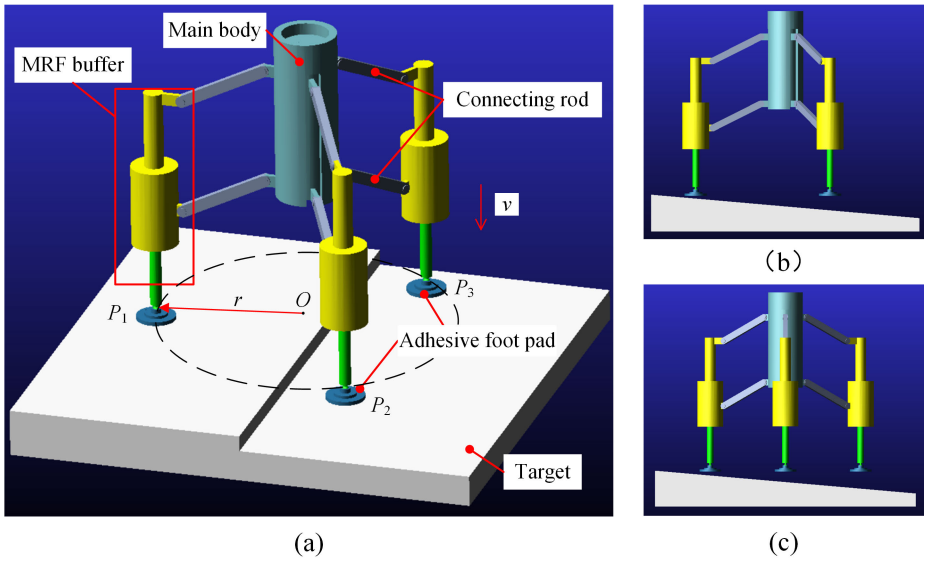

FIGURE 9. Schematic diagram of multi-adhesive foot structure and impact conditions: (a) impact step with 1-2 condition, (b) impact slope with 1-2 condition, (c) impact slope with 1-1-1 condition.

TABLE 3. Simulation conditions.

Test No.	Target surface characteristics	Impact velocity (m/s)	Impact condition
1	Step (Height: 20 mm)	3.5	1-2
2	Slope (Inclination: 5°)	3.5	1-2
3	Slope (Inclination: 5°)	3.5	1-1-1

above 1000 N, see Figure (b), but soon the postures of the foot pads adjust passively under the action of the spherical joint and the contact force decreases.

In the impact process, according to the fuzzy control rules previously designed, the controller adjusts the buffer active damping force F_a in real time, see Fig. 10 (a), making the contact forces between three adhesive food pads and the target always more stable at 300 N which meets the design requirements. The buffer stroke of P1 reaches 97 mm, close to the buffer limit of 100 mm, and that of the other two are 75.746 mm. The difference is $\Delta s = 20.005$ mm, equal to the height of the step.

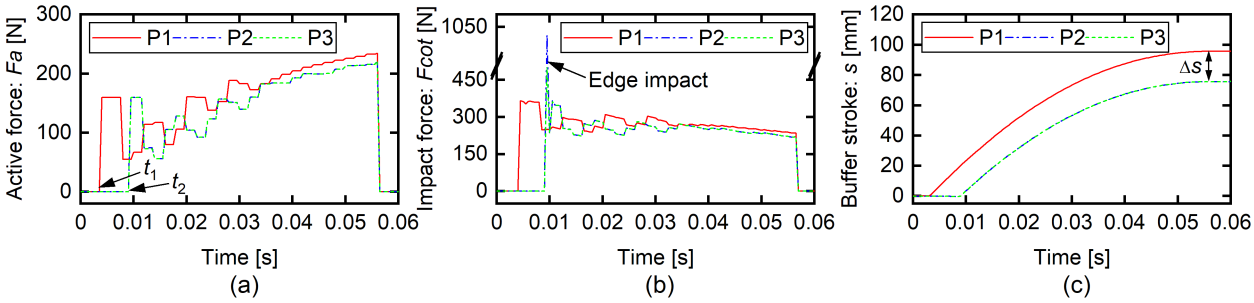

FIGURE 10. Simulation results of step impact process with 1-2 condition. (a) Active damping force F_a, (b) impact force F_{cot}, (c) buffer stroke s (Test 1).

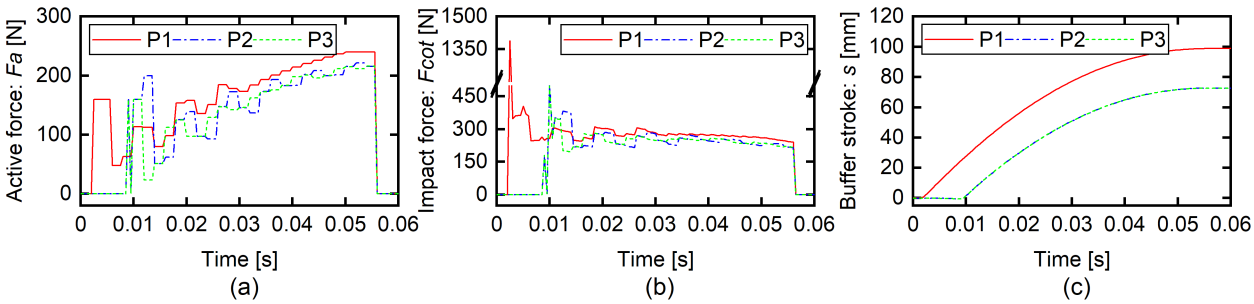

FIGURE 11. Simulation results of slope impact process with 1-2 condition. (a) Active damping force F_a, (b) impact force F_{cot}, (c) buffer stroke s (Test 2).

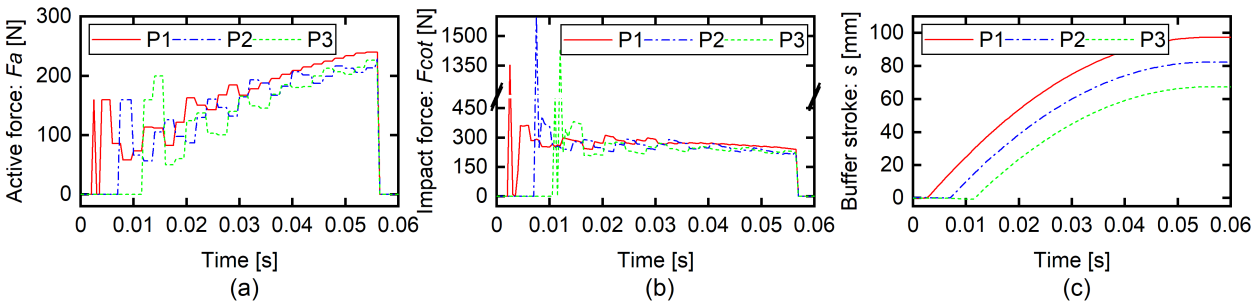

FIGURE 12. Simulation results of slope impact process with 1-1-1 condition. (a) Active damping force F_a, (b) impact force F_{cot}, (c) buffer stroke s (Test 3).

The simulation results of slope impact process with 1-2 and 1-1-1 conditions are shown in Fig. 11 and Fig. 12. As it is a tilted collision, the edge effect causes a transient peak in the collision force of all three adhesive feet in contact with the target. Similar to the result of Test 1, due to the real-time adjustment of the buffer damping, the contact force F_{cot} between each foot and the target can be controlled around 300 N both in Test 2 and Test 3. It can be clearly seen from Fig.12 (b) that although the impact times of the three adhesive feet and the target are different, the contact forces of the three feet are almost the same in the whole impact process due to the fuzzy controller. The buffer strokes of three adhesive feet are 97.490 mm, 82.508 mm and 67.50 mm respectively.

VI. CONCLUSION

This paper presents a space debris adhesion capture method. The device can be launched from a satellite platform and attached to the debris surface through impact to achieve the purpose of capture. It provides the advantages of standoff distance allowed, high compatibility with different shaped targets and almost no risk of generating new debris. A single-adhesive foot device is designed with gecko adhesive material at the end, and the body is a variable damping MRF buffer. The basic parameters of the device and the buffer are designed, and the active and passive damping force are determined. Moreover, a fuzzy control method with impact force and buffer stroke as the inputs and active damping force as the output is also established for impact process preload

controlling. Based on Adams and Simulink, co-simulations are carried out and the results show that the device proposed is able to stabilize the contact force within a set value by adjusting the buffer damping force in real time during impact process, thus providing appropriate preload for the adhesive foot pad. Multi-adhesive foot structure is also discussed and demonstrates its reliability and adaptability on complex impact conditions.

Nevertheless, much research work remains to be done in future. The actuated detachment method and mechanism need to be designed to make the device has the ability to be retrieved and then performed the next debris capture task. Also, collision process dynamics modelling analysis is required to determine the impact effects on debris target attitude and a large number of ground experiments need to be carried out to verify the feasibility and reliability.

REFERENCES

[1] A. Murtaza, S. J. H. Pirzada, T. Xu, and L. Jianwei, "Orbital debris threat for space sustainability and way forward (review article)," *IEEE Access*, vol. 8, pp. 61000–61019, Jan. 2020.

[2] M. Shan, J. Guo, and E. Gill, "Review and comparison of active space debris capturing and removal methods," *Prog. Aerosp. Sci.*, vol. 80, pp. 18–32, Jan. 2016.

[3] B. Xu, Y. Yang, B. Zhang, Y. Yan, and Z. Yi, "Bionic design and experimental study for the space flexible webs capture system," *IEEE Access*, vol. 8, pp. 45411–45420, 2020.

[4] Q. Chen, G. Li, Q. Zhang, Q. Tang, and G. Zhang, "Optimal design of passive control of space tethered-net capture system," *IEEE Access*, vol. 7, pp. 131383–131394, 2019.

[5] K. Takahashi, C. Charles, R. W. Boswell, and A. Ando, "Demonstrating a new technology for space debris removal using a bi-directional plasma thruster," *Sci. Rep.*, vol. 8, no. 1, pp. 1–10, Dec. 2018.

[6] R. Dudziak, S. Tuttle, and S. Barraclough, "Harpoon technology development for the active removal of space debris," *Adv. Space Res.*, vol. 56, no. 3, pp. 509–527, Aug. 2015.

[7] G. S. Aglietti *et al.*, "RemoveDEBRIS: An in-orbit demonstration of technologies for the removal of space debris," *Aeronaut. J.*, vol. 124, no. 1271, pp. 1–23, Jan. 2020.

[8] J. L. Forshaw, G. S. Aglietti, S. Fellowes, T. Salmon, I. Retat, A. Hall, T. Chabot, A. Pisseloup, D. Tye, C. Bernal, F. Chaumette, A. Pollini, and W. H. Steyn, "The active space debris removal mission RemoveDebris. Part 1: From concept to launch," *Acta Astronautica*, vol. 168, pp. 293–309, Mar. 2020.

[9] J. Reed and S. Barraclough, *Development of Harpoon System for Capturing Space Debris*. Paris, France: Esa Special, 2013.

[10] A. Bylard, R. MacPherson, B. Hockman, M. R. Cutkosky, and M. Pavone, "Robust capture and deorbit of rocket body debris using controllable dry adhesion," in *Proc. IEEE Aerosp. Conf.*, Mar. 2017, pp. 1–9.

[11] Y. Li, J. Krahn, and C. Menon, "Bioinspired dry adhesive materials and their application in robotics: A review," *J. Bionic Eng.*, vol. 13, no. 2, pp. 181–199, Jun. 2016.

[12] H. Jiang, E. W. Hawkes, C. Fuller, M. A. Estrada, S. A. Suresh, N. Abcouwer, A. K. Han, S. Wang, C. J. Ploch, A. Parness, and M. R. Cutkosky, "A robotic device using gecko-inspired adhesives can grasp and manipulate large objects in microgravity," *Sci. Robot.*, vol. 2, no. 7, Jun. 2017, Art. no. eaan4545.

[13] D. Paretkar, M. Kamperman, A. S. Schneider, D. Martina, C. Creton, and E. Arzt, "Bioinspired pressure actuated adhesive system," *Mater. Sci. Eng., C*, vol. 31, no. 6, pp. 1152–1159, Aug. 2011.

[14] J. Purtov, M. Frensemeier, and E. Kroner, "Switchable adhesion in vacuum using bio-inspired dry adhesives," *ACS Appl. Mater Interface*, vol. 7, Nov. 2015, Art. no. 24127.

[15] P. Kowol, "From simple experiments to modern mechatronic devices-development of MR fluid applications," in *Proc. Sel. Problems Electr. Eng. Electron. (WZEE)*, Sep. 2015, pp. 1–4.

[16] M. Ashtiani, S. H. Hashemabadi, and A. Ghaffari, "A review on the magnetorheological fluid preparation and stabilization," *J. Magn. Magn. Mater.*, vol. 374, pp. 716–730, Jan. 2015.

[17] C. Wang, H. Nie, J. Chen, and H. P. Lee, "The design and dynamic analysis of a lunar lander with semi-active control," *Acta Astronautica*, vol. 157, pp. 145–156, Apr. 2019.

ZHENGYOU XIE received the Ph.D. degree in mechanical engineering from the Harbin Institute of Technology, Harbin, China, in 2019. He is currently a Postdoctoral Researcher with the Qian Xuesen Laboratory of Space Technology, Beijing, China. His current research interest includes space debris removal technology.

XINLONG CHEN received the Ph.D. degree in aircraft design from the Harbin Institute of Technology, Harbin, China, in 2008. He joined the China Academy of Space Technology, Beijing, China. He is currently a Professor with the Qian Xuesen Laboratory of Space Technology, China Academy of Space Technology. He is also the Director of the Research Center of Space Debris Removal. His research interests include overall design and research of spacecraft in space security and in-orbit services.

YAJING REN received the M.A. degree in translation and bilingual communication from Hong Kong Baptist University, China, in 2017. She joined the Qian Xuesen Laboratory of Space Technology, Beijing, China, in 2018. She is currently an Engineer with a focus on intelligence research.

YANGYANG ZHAO received the B.S. degree in mechanical design, manufacturing and automation from Zhejiang Sci-Tech University, China, in 2018. From 2018 to 2020, he worked as a Fixture Engineer with Zhejiang Tianzheng Electric Company Ltd., China. He joined the Qian Xuesen Laboratory of Space Technology, Beijing, China, in 2020. His research interests include novel aerospace product design and development.